Energy, Mines and Resources Canada

Énergie, Mines et Ressources Canada

CANMET

Canada Centre for Mineral and Energy Technology

Centre canadien de la technologie des minéraux et de l'énergie

Mining Research Laboratories

Laboratoires de recherche minière

Canada

WAVEFORM ANALYSIS AND VELOCITY STRUCTURE AT QUIRKE MINE AND ADJACENT AREAS PART 1: SOURCE PARAMETERS FOR EVIDENCE OF THE FAILURE ZONE

SHENGZAO CHEN AND D.G.F. HEDLEY

MRL 90-117 (TR) JULY 1990

This document is an unedited interim report prepared primarily for discussion with selected report partners. It does not represent a final expression of the opinion of the Canada Centre for Mineral and Energy Technology (CANMET)

Ce document est un rapport provisoire non-révisé et rédigé principalement pour la discussion et la documentation interne. Il ne représente nullement l'expression définitive de l'opinion du Centre canadien de la technologie des minéraux et de l'énergie (CANMET)

39 pp

MICROMEDIA

91-01034/

WAVEFORM ANALYSIS AND VELOCITY STRUCTURE AT QUIRKE MINE AND ADJACENT AREAS PART 1: SOURCE PARAMETERS FOR EVIDENCE OF THE FAILURE ZONE

Shengzao Chen* and D.G.F. Hedley**

ABSTRACT

The spectral analyses of 37 rockbursts recorded at Quirke Mine during 1987 were carried out. The seismic energy of E_P to E_T is 22%, higher than in South African gold mines (i.e., 10%). The higher P-wave energy at Quirke Mine could be due to the predominant pillar bursting mechanism at that mine. The stress drop is determined between 100 kPa and 5 MPa which is similar to those of 500 kPa and 5 MPa in South African gold mines, but with a lower bottom limit at Quirke. Peak particle velocities (PPV) of 37 events and accelerations (PPA) of 18 events were evaluated. The product of R, distance from source, and V, PPV, against magnitude, Mn, has a relationship Log(RV) = 0.60 Mn - 1.33, which is in good agreement with the adjacent Denison Mine, and also Creighton and Strathcona Mines in Northern Ontario. The relationships between different source parameters for both P and S-waves were analyzed and compared with others in Canada and different areas in the world.

Key words: Rockburst; Waveform analysis; Source parameter; Seismic velocity

*Post-Doctoral Fellow, Elliot Lake Laboratory, CANMET, Energy, Mines and Resources Canada, Elliot Lake, Ontario, visiting from State Seismological Bureau, China.

**Research Scientist, Elliot Lake Laboratory, CANMET, Energy, Mines and Resources Canada, Elliot Lake, Ontario.

ANALYSE DES FORMES D'ONDE ET STRUCTURE DE VITESSE À LA MINE QUIRKE ET DANS LES ENVIRONS PARTIE 1: LES PARAMÈTRES DE SOURCE, INDICATEURS DE LA ZONE DE RUPTURE

Shengzao Chen* et D.G.F. Hedley**

RÉSUMÉ

Les analyses spectrales de 37 coups de toit enregistrés à la mine Quirke en 1987 ont été effectuées. Le rapport des énergies sismiques E_P/E_T est plus élevé (22 %) que dans les mines d'or d'Afrique du Sud (10 %). L'énergie des ondes P plus élevée à la mine Quirke tiendrait au mécanisme prédominant d'éclatement des piliers dans cette mine. La chute des contraintes varie entre 100 kPa et 5 MPa, ce qui se compare aux valeurs de 500 kPa et de 5 MPa dans les mines d'or d'Afrique du Sud, la limite inférieure étant plus faible à la mine Quirke. Les vitesses maximales des particules (VMP) de 37 événements et les accélérations maximales des particules (AMP) de 18 événements ont été évaluées. Le produit de R, la distance de la source, et de V, VMP, est relié à la magnitude, Mn, par l'équation log(RV) = 0,60 Mn - 1,33, ce qui corrobore les données pour la mine voisine Denison et aussi celles pour les mines Creighton et Strathcona dans le nord de l'Ontario. Les relations entre différents paramètres de source autant pour les ondes P que pour les ondes S ont été analysées et comparées à d'autres relations relevées au Canada et dans différentes régions dans le monde.

Mots clés: coup de toit; analyse des formes d'onde; paramètre de source; vitesse sismique

*Boursier post-doctoral du Bureau sismologique d'État, Chine, invité au Laboratoire d'Elliot Lake, CANMET, Énergie, Mines et Ressources Canada, Elliot Lake (Ontario).
**Chercheur scientifique, Laboratoire d'Elliot Lake, CANMET, Énergie, Mines et Ressources Canada, Elliot Lake (Ontario).

CONTENTS

	Page
ABSTRACT	i
RESUME	ii
INTRODUCTION	1
DATA PROCESSING	1
WAVEFORM ANALYSIS IN FREQUENCY DOMAIN	1
Seismic Energy	3
Seismic Moment	5
Corner Frequency and Source Radius	7
Stress Drop	9
Peak Particle Velocity (PPV) and Acceleration	11
DISCUSSION	13
CONCLUSIONS	14
ACKNOWLEDGEMENTS	15
REFERENCES	15

TABLES

1.	List of rockburst events in Quirke Mine	2
2.	Responses at each site	13

FIGURES

1.	Plan view of Quirke Mine showing extent of failed zone, sensor and seismic event locations	20
2.	A stereogram of rockburst event locations at Quirke Mine and its adjacent areas in 1987	21
3.	Proportion of seismic energy in P-wave at Quirke Mine	22
4.	Seismic energy as a function of magnitude at Quirke Mine	23
5.	Relationship between seismic energy and magnitude	24
6.	Relationship between the seismic moments for P- and S-waves at Quirke Mine and adjacent areas	25
7.	Relationship between seismic moment and magnitude at Quirke and Strathcona mines	26
8.	Relationship between the source radius for P- and S-waves at Quirke Mine	27

9. Relationship between P- and S-wave corner frequencies in the seismic spectra at Quirke Mine 28

10. Seismic moment as a function of corner frequency at Quirke Mine 29

11. Relationship between stress drops for P- and S-waves at Quirke Mine. 30

12. Relationship between the peak particle velocities for P- and S-waves at Quirke Mine 31

13. Scaled peak particle velocity as a function of rockburst magnitude, using a seismology format 32

14. Relationship between the peak particle accelerations for P- and S-waves at Quirke Mine 33

15. Log(Ωo) as a function of f_o at Quirke Mine 34

INTRODUCTION

Quirke Mine has a history of rockbursts dating back to 1982. Hedley (1) has investigated the progressive failure of a section of the mine, see Figure 1. The instrumentation used to monitor seismicity at Quirke Mine has been described by Labuc (2), and a preliminary study of waveform analysis has been done by Semadeni et al. (3). In order to reveal the detailed features of the failure zone in the hanging wall a systematic study of waveform analysis with both geophones and accelerometers was carried out. The seismic velocity structures of P- and S-waves recorded by 5 sensors (Figure 1) were used to evaluate the failure zone, as well as waveform analysis in frequency domain. These analyses and geological interpretation will contribute to a better understanding of rockburst mechanisms.

DATA PROCESSING

Thirty-seven rockburst events in 1987 (Table 1) ranged from 0.7 to 2.3 in magnitude, Mn. The hypocenters have been relocated using residual time contours (see part 2 of this report) and/or the Block Program used in this laboratory to determine the velocity structure at the mine. The location of seismic events are shown on a stereogram in Figure 2. Digitized signals from each axis (x, y, z) of five sensors for these events were analyzed to obtain the source parameters. Analysis of source parameters was completed in frequency domain using the Brune model (4,5). All analyses were done interactively using colour graphics with operator input from a mouse.

WAVEFORM ANALYSIS IN FREQUENCY DOMAIN

Spectral analysis of seismic waveforms in the frequency domain is used in seismology to obtain information on source mechanisms and dimensions. Brune (4) proposed a relatively simple circular fault model that affords tractable expressions for calculating some of the faulting parameters. This

Table 1 - List of rockburst events in Quirke Mine
(Events 1 through 18 recorded using accelerometers)

Event (No.)	Date	Time	Magnitude (Mn)	Event (No.)	Date	Time	Magnitude (Mn)
1	27/03/87	00:01:05	0.7	20	28/08/87	03:35:00	1.6
2	16/04/87	18:26:06	1.1	21	28/08/87	07:40:51	1.4
3	17/04/87	14:39:56	1.2	22	28/08/87	07:53:48	0.8
4	17/04/87	15:27:59	0.7	23	29/08/87	07:46:55	2.3
5	18/04/87	02:51:50	1.4	24	04/09/87	15:36:07	0.8
6	19/04/87	07:19:05	0.7	25	05/09/87	19:03:07	0.9
7	19/04/87	09:41:17	1.7	26	06/09/87	07:58:33	1.2
8	25/04/87	13:04:27	0.8	27	06/09/87	07:59:20	0.9
9	26/04/87	23:50:41	0.7	28	09/09/87	06:22:28	1.2
10	29/04/87	01:13:24	0.8	29	08/10/87	17:04:06	1.4
11	02/05/87	15:47:27	0.7	30	15/10/87	00:50:53	1.1
12	02/05/87	16:58:45	0.8	31	24/11/87	07:16:55	2.1
13	06/05/87	04:48:34	0.7	32	24/11/87	18:45:45	1.8
14	07/05/87	20:06:14	1.1	33	24/11/87	18:50:46	0.8
15	07/05/87	20:47:54	0.7	34	29/11/87	07:29:29	1.8
16	09/05/87	07:33:01	0.7	35	18/12/87	23:51:14	1.9
17	17/05/87	05:44:26	0.8	36	19/12/87	09:43:07	1.0
18	21/05/87	17:46:38	1.0	37	09/12/87	22:03:24	1.7
19	28/08/87	01:07:54	0.9				

is the most commonly used model for earthquakes and mining-induced seismic events. The mechanics of slippage on the fault with a circular area have been developed in rock mechanics by Salamon (6).

The seismic signals in the form of a displacement wave are transformed into a frequency distribution using Fast Fourier Transform technology. Hanks (7) and Wyss (8) tested the procedure on two earthquakes, for which other estimates of fault size are available, and found that the Brune model yielded results for both earthquakes in reasonable agreement with the independent estimates. The spectrum of the far-field displacement radiation from a conventional fault model (9) and Berckhemer-Jacob model (10) has been calculated for comparison with the spectrum calculated from the Brune model. It was demonstrated that the spectra were generally similar, but some of the details were attributed to different effects in the two models (11).

The calculated seismic moment is an independent measure of the magnitude of the event based on the far-field radiation pattern. Other parameters of the fault dimension are dependent on the type of model used, in which the main discrepancies seem to be due to the uncertainty of the estimates of corner frequencies, especially for S-waves (12-16). The following results and interpretations are based on Brune (4) and Trafunac (17) models.

SEISMIC ENERGY

The total elastic energy radiated from a point source in an elastic medium can be expressed (18) by:

$$E_T = 4\pi R^2 \rho \left(\alpha \int^{T_\alpha} V_\alpha^2 \, dt + \beta \int^{T_\beta} V_\beta^2 \, dt\right) \qquad \text{Eq 1}$$

where, R = distance from sensor to source

α and β = velocity of P- and S-wave, respectively

ρ = rock density (2700 kg/m^3)

V_α and V_β = particle velocity (ground motion velocity) in P- and S-wave

T_α and T_β - duration of seismic waves in P and S phases.

Triaxial geophones with 3 sensors mounted orthogonally record the total seismic energy liberated.

The ratio of energy in the P-wave to the total energy, E_P/E_T, is about 0.22 at Quirke Mine, i.e., around 80% of the total energy is contained in the S-wave (Figure 3). This is consistent with observations for mine tremors in South Africa (18,19), but typically it was found that only about 10% of the seismic energy was contained in the P-wave (20). From these observations it was concluded that shear is the predominant failure mechanism. At Quirke Mine the high P-wave energy can be primarily related to the pillar bursting mechanism.

As shown in Figure 3, the energy values include those calculated from accelerometer events (No. 1-18 in Table 1) which were not evaluated by Semadeni (3).

The relationship between seismic energy and magnitude for Quirke Mine alone (Figure 4) can be expressed by:

$$\text{Log } (E_T) = 1.72\ Mn + 0.59 \qquad \text{Eq 2}$$

Eliminating the accelerometer recorded events and using all of the 19 velocity gauge events in Figure 2, the relationship can be expressed by:

$$\text{Log}(E_T) = 1.54\ Mn + 0.61 \qquad \text{Eq 3}$$

which is consistent with the Strathcona Mine and has the same slope value as in McGarr's statistical relationship (Figure 5).

Equation 3 has a broader application because of the events with a large magnitude range of 0.8 - 2.7 Mn. It can be determined that at Quirke Mine, with a magnitude range of Mn <2.0 (0.7 - 1.9), the seismic energy increases faster with magnitude than in the Strathcona Mine, with a magnitude range of Mn >2.0. Meanwhile, Equation 3 is similar to the linear relationship for tremors in a deep-level gold mine at ERPM in South Africa (19), which was used by McGarr (21) to study seismic moments and volume changes. Primary results

on the variation of seismic energy with magnitude at Quirke Mine and Strathcona Mine are comparable with the ERPM gold mine.

Considering the effect of distance from source to array on energy-magnitude relationships, the slope of Equation 3, with a lower intercept of about 0.6, is closer in the case of a nearby array by:

$$\text{Log}(E_T) = 1.55\ Mn + 1.2 \qquad \text{Eq 4}$$

which is shown by Semadeni (3) under the line of Gutenberg (22). It is evident that the trend of Equation 2 intersects all those mentioned above at almost the same intercept as for Equation (3), and has a steeper slope. This implies that a higher seismic energy occurred at Quirke Mine.

SEISMIC MOMENT

The basic use of the concept of seismic moment is to estimate the average stress at the seismic source. Aki (23) and Brune (24) suggested that spectrum fitting to determine the absolute stress was equivalent to the energy/moment ratio method. The magnitude of the plateau is a measure of the energy of the seismic event and is related to the seismic moment as follows:

$$Mo = \frac{4\pi\rho C^3\ R\Omega_o}{f^c r^c} \qquad \text{Eq 5}$$

where, Ω_o = low frequency plateau

ρ = rock density

C = velocity of either P-wave, α, or S-wave, β

R = distance from source to sensor

f^c = radiation pattern coefficients

r^c = free-surface effects (for surface sensors only).

In seismology, usually only the seismic moment from the SH wave is calculated since the surface effects are known and constant. The radiation coefficients are assigned average values of 0.39 for P-waves, and 0.57 for S-waves. The free-surface effects, r^c, are ignored as they are only used for surface sensors. The velocity of P- and S-waves are respectively taken as α =

5940 m/s, and β = 3660 m/s at Quirke Mine, which have been verified as valid in our studies of hypocenter determinations. The final results of the seismic moment for each site were combined as vector sums.

Using f^c = 0.39 and 0.57 for P- and S-waves, respectively, the ratio of Mo^P/Mo^S is 0.72 for 28 events, eliminating events 19-23, 28, 31, 34 and 35 from Table 1, and 0.94 for 37 events (Figure 6). Assuming Mo is the same for each station we find that the coefficient f^c is close to 0.57, with a range of 0.35 to 0.64 which implies the different responses from each sensor site. One may well say that f^c = 0.39 is used to calculate the seismic moments for the P-wave, and that f^c = 0.57 is used to measure the seismic moments for the S-wave at Quirke Mine.

The relationship between seismic moment and magnitude can be expressed by:

$$\text{Log(Mo)} = 0.53\ \text{Mn} + 1.89 \qquad \text{Eq 6}$$

for 37 events at Quirke Mine and adjacent areas. This relationship is in close agreement with the result obtained by Semadeni (3).

Just using the velocity gauge recorded events gives:

$$\text{Log(Mo)} = 1.0\ \text{Mn} + 1.22 \qquad \text{Eq 7}$$

which is in line with Strathcona Mine (Figure 7), and closer to the relationship of Log(Mo) = 0.94 Mn + 1.32, described by Hasegawa (25) for earthquakes in the Canadian Shield.

Semadeni et al. (3) assumed their empirical relationship with a lower slope and a higher intercept than Hasegawa's trend line was due to the insufficient time window of 0.8 sec. As we know, the interpretation of statistical results of any kind of physical variables is rarely unique, and it always has error ranges in a specific data field, not to mention dependence on the physical models used. The calculated seismic moments and the empirical relationships between seismic moment and magnitude as determined here are valid enough to be used.

CORNER FREQUENCY AND SOURCE RADIUS

The corner frequency (f_o) indicates the intersection of the plateau (Ωo), the low frequency trend parallel to the frequency axis, and the high frequency decay in the spectrum. It is a very common seismological observation that P-waves are enriched in high-frequency motion relative to the S-waves recorded for the same earthquake. The obs rved fact in the seismic spectra that P-wave corner frequency is typically greater than the S-wave corner frequency is called the corner frequency shift. Molnar (26) calculated the spectra of body waves radiated from a realistic model of a circular fault. Using this model they were able to manifest the corner frequency shift, thereby resolving an apparent discrepancy between some theoretical studies (11, 13) and observations.

The source radius is related to the corner frequency by:

$$r_o = \frac{2.34\,\beta}{2\pi f^S_o} \qquad \text{Eq 8}$$

for S-waves (4), and

$$r_o = \frac{1.97\,\alpha}{2\pi f^P_o} \qquad \text{Eq 9}$$

for P-waves (16).

Assuming r_o constant we have:

$$\frac{f^P_o}{f^S_o} = \frac{1.97\,\alpha}{2.34\,\beta} \qquad \text{Eq 10}$$

If $\alpha/\beta = \sqrt{3}$, then $f^P_o/f^S_o = 1.46$.

At Quirke Mine $\alpha/\beta = 5940/3660 = 1.62$, hence, $f^P_o/f^S_o = 1.36$ which is normal.

Generally, if $f^P_o/f^S_o < 1.46$, then $\alpha < \sqrt{3}\beta$, i.e., low P-wave velocity; if $f^P_o/f^S_o > 1.46$, then $\alpha > \sqrt{3}\beta$, i.e., low S-wave velocity.

The ratio of r^P_o/r^S_o is 0.84 for 28 events (Figure 8), and 0.94 for 37 events, which is nearly consistent with theoretical analysis and assumed conditions. These conditions explain that the higher ratio of f^P_o versus f^S_o

(over 1.46) existed at the mine. From Equations 8 and 9, we have a general relationship: $r^P_o/r^S_o = 0.84\ (\alpha/\beta)/(f^P_o/f^S_o)$. Only when $f^P_o/f^S_o = 1.46$, there exists $r^P_o/r^S_o = 1$ for $\alpha = \sqrt{3}\beta$.

The spectral analysis of rockbursts at Quirke Mine reveals a general tendency for an average ratio of $f^P_o/f^S_o = 1.69$ (Figure 9), which is characterized by lower S-wave velocities. Similarly, most observations indicate $f^P_o/f^S_o > 1$, e.g., the ratio 1.0 - 1.7 in Japan (27), 1.5 in the USSR (28), 1.7 in Oroville, California (29), and 2.0, the highest ratio so far, in the Himalayan region (30). A similar tendency of f^P_o/f^S_o was also observed on the Burma-India border (31), and in Greece (32).

The corner frequency shift is a very common observation, even though some anomalous results were found in different tectonic circumstances, such as $f^P_o/f^S_o = 0.96 \pm 0.17$ for 18 earthquakes along, or through, the relatively low-loss Sierra batholith (33). No corner frequency shift was observed for 24 mining-induced tremors at ERPM, South Africa (19), which were similar to earthquakes of true tectonic origin, seismogenic failure. Also, $f^S_o > f^P_o$ was observed for 26 earthquakes along the San Andreas fault (34). Some unusual wave propagation effects seem likely to have affected the results.

It is supposed to be a source property if the corner frequency shift results only from a sort of source finiteness effects distinctly different from conventional Haskell-type dislocation models. However, the observational results are very scattered and it is necessary to find other ways to interpret these phenomena. The matter can be put in several ways, but basically it involves the wave propagation effects, including an elastic attenuation (35), elastic scattering (13), and the crustal structure (36). Most of the spectral studies reporting a corner frequency shift present observations in the range of 1.2 to 1.7. Similar observations were obtained at Quirke Mine.

The smaller number of f^P_o/f^S_o observations ($\leq$1.1 to 1.2) obviously does not lead to a report of the shift. An even smaller number of observations for

f^P_o/f^S_o >1.7, obtained at Quirke Mine, are hard to understand as a source effect alone. Wave propagation effects seem to be an explanation, but then it is also true that such effects, to at least some extent, could affect all the observations and not only for those of f^P_o/f^S_o >1.7. This has been recognized by Hanks (15). Undoubtedly for Quirke Mine the crustal structure effects can be ignored since the seismic focus at about 500 m depth is very shallow.

It is worth emphasizing that the corner frequency f_o discussed here, not f_c defined by Silver (16), appears to be primarily controlled by critical events in the rupture history of the source such as nucleation, abrupt changes in rupture velocity, and complete termination of motion (37,38). In this regard, the corner frequency shift observations at Quirke may be associated with pillar bursts or mining-induced burst events, and to some extent may be related to the pillar implosion. At ERPM in South Africa, the underground observations of damage caused by large tremors indicate that the actual rupture process is highly complex, consisting of many discrete failures which cannot be fitted by a simple dislocation model (19). It appears that when slippage suddenly occurs along a geological weakness plane, a fault-slip burst, the third classification of rockbursts as summarized by Hedley (20), is produced. This type of fault-slip events have the same mechanism as an earthquake and may be compared with the central California earthquakes along the San Andreas Fault. That is why such a difference in the observations of f^P_o/f^S_o is displayed between Quirke Mine and ERPM in South Africa, and central California along the San Andreas Fault.

STRESS DROP

The contour lines of constant stress drops can be drawn on a double logarithm plot of seismic moment versus corner frequency, following the relationship:

$$\text{Log}(Mo) = \text{Log}(\frac{16}{7}\Delta\sigma) + 3\ \text{Log}\ (\frac{2.34\beta}{2\pi f_o}) \qquad \text{Eq 11}$$

The present results indicated that all of both 28 and 37 events at Quirke and neighbouring areas fell between the constant stress drop lines of 100 kPa and 5 MPa despite the fact that both f^c = 0.57 or 0.39 and r_o = $2.34\alpha/(2\pi f_o)$ or r_o = $1.97\alpha/(2\pi f_o)$ were used for P-waves, based on the same parameters f^c = 0.57 and r_o = $2.34\beta/(2\pi f_o)$ for S-waves. This means the stress drop is more or less independent of the seismic moment.

For large earthquakes, the typical values of constant stress drop are 1 to 10 MPa (20). As shown in Figure 10, the upper limit of 5 MPa is located in this value range but the lower limit is much less than 1.0 MPa because of the low magnitudes of 0.7 or less than 1.0 Mn yielding the low corner frequency and plateau.

For a number of mine tremors at ERPM in South Africa most events fell between the constant stress drop lines of 500 kPa and 5 MPa (19,39). In Southern California the vast majority of earthquakes yielded stress drops in the range of 100 kPa to 100 MPa, and there was no consistent variation of stress drop with seismic moment (40). The higher stress drop seems to be relevant to the large seismic moment and/or low corner frequency. Our results strongly support those from Semadeni (3), and are similar to a great extent to those from the Strathcona Mine (20). A similar observation has been made for small mine tremors in Polish copper mines (41). All these results imply that corner frequency decreases and source radius increases with increasing seismic moment conditional on the constant stress drop.

For a Poisson's ratio of 0.25, the Salamon model (6) reduces to the Brune model and yields the stress drop:

$$\Delta\sigma = \frac{7M_o}{16r_o^3} \qquad \text{Eq 12}$$

From this equation it appears that the stress drop increases with decreasing source radius or rather increasing corner frequency, and with increasing seismic moment. Using Equation 11, we can draw a group of constant stress drop lines which are parallel to each other, and in which the constant values

are increasing from the left lower corner of the plot to the increasing direction of seismic moment and corner frequency. In various areas for different groups of earthquakes, the seismic moments - corner frequencies may be distributed in different divisions. These are limited to between two lines of constant stress drop on the plot, and hence the classification of earthquakes may well be derived from this.

The ratio of stress drop for P- and S-waves can be estimated as follows:

$$\frac{\Delta\sigma_P}{\Delta\sigma_s} = \frac{Mo^P}{Mo^s} \left(r^P{}_o / r^S{}_o\right)^{-3} \qquad \text{Eq 13}$$

Substituting the yielded results on Mo and r_o for P- and S-waves into Equation 13 we obtain:

$$\frac{\Delta\sigma_P}{\Delta\sigma_s} = 1.2$$

for 28 events at Quirke Mine, and

$$\frac{\Delta\sigma_P}{\Delta\sigma_s} = 1.1$$

for 37 events at Quirke and its adjacent areas. These ratios are in close agreement.

However, when directly using the calculated stress drops to estimate the ratio of $\Delta\sigma_P/\Delta\sigma_s$, it is only 0.79 and 0.73, for 28 and 37 events, respectively (Figure 11). These discrepancies must be related to: 1) statistical errors since the calculated stress drops are scattered, and 2) propagation effects including an elastic attenuation and elastic scattering caused by the fractured nature of rock mass at Quirke Mine.

PEAK PARTICLE VELOCITY (PPV) AND ACCELERATION

All PPV of 37 events are calculated and the relationships between V_{PP} and V_{PS} for P- and S-waves are expressed by:

$$V_{PP} = 0.546\ V_{PS} - 0.005 \qquad \text{Eq 14}$$

which is shown in Figure 12 for 28 events at Quirke, and

$$V_{PP} = 0.53\ V_{PS} + 0.001 \qquad \text{Eq 15}$$

for 37 events at Quirke and adjacent areas.

Neglecting the intercept terms in Equations 14 and 15, we can obtain a mean ratio of V_{PP}/V_{PS} of about 0.54 ± 0.01 in the Quirke area. This agrees with the basic principle that the PPV of the S-wave is greater than the P-wave.

Since peak particle velocity is strongly related to distance from source, we use the product of R and PPV to find the relationship with magnitude (Mn), expressed by:

$$\text{Log(RV)} = 0.60\ \text{Mn} - 1.33 \qquad \text{Eq 16}$$

for S-waves, and

$$\text{Log(RV)} = 0.71\ \text{Mn} - 1.65 \qquad \text{Eq 17}$$

for P-waves at Quirke Mine.

Figure 13 shows the results of 37 events from Quirke Mine combined with results from other mines in Ontario. Hedley (42) gave the relationship of Log(RV) = 0.63 M - 1.33 for Creighton, Strathcona, Quirke and Denison, which is very close to the present result as shown in Equation 16.

Peak particle velocities from 37 rockbursts at Quirke indicated that measured velocities are considerably lower than those measured in South African gold mines for comparable magnitudes and distances, in which different magnitude scales are used, i.e., Nuttli's in eastern North America, and Richter's in South Africa. This further confirmed the analysis of the observations from the 17 events at Quirke and adjacent Denison (41).

For the first time peak particle accelerations (PPA) for 18 accelerometers recorded events at Quirke Mine have been analyzed. The calculated results of PPA show a range of 3.59 to 126.65 mm/s^2 for P-waves, and 5.07 to 170.34 mm/s^2 for S-waves. The relationship between A_p for P-waves, and A_s for S-waves at Quirke can be expressed (Figure 14) by:

$$A_p = 0.54\ A_s + 2.00 \qquad \text{Eq 18}$$

which is nearly parallel to the trend of V_{PP} -V_{SS} with a similar slope of about 0.54. It is also a common feature that all values of A_s are greater than A_p.

DISCUSSION

Due to heterogeneity of the rock mass around the rockburst zone at Quirke Mine, different responses of each sensor site may arise in observations. Assuming Mo to be constant for each site and for both the P- and S-waves, and especially assuming site 1 has radiation coefficients of 0.39 and 0.57, it was found that for f^c = 0.39 the coefficients of f^c for other sites appear to be too high. For f^c = 0.57 at site 1, the other responses are shown in Table 2.

Assuming the source radius is constant for P- and S-waves and for different sites, and taking $r_o = \kappa\beta/f_o$, the responses for constant κ at each site will be seen (Table 2).

Table 2 - Responses at each site (from 22 events at Quirke Mine)

Site	1	2	3	4	5
f^c	0.57	0.35	0.57	0.64	0.39
κ	0.37	0.31	0.23	0.27	0.33

Since we have assumed β and r_o are constant, κ is only dependent on f_o. The average corner frequencies for 22 events are f_o = 40, 35, 41 at sites 1, 3 and 4, and 48 and 51 at sites 2 and 5, respectively. The inverse proportional relationship between κ and f_o is in good agreement except for site 1 for which we forced κ as 0.37 to make r_o constant. Combining these responses of f^c, κ, and f_o, all five sites are divided into two groups: group 1 consisting of sites 1, 3 and 4, and group 2 consisting of sites 2 and 5.

Figure 15 shows the relationship between logarithmic plateau and corner

frequency of different sensor sites in Quirke Mine. Geophones 1, 3 and 4 have a very similar trend of function $\log(\Omega o)(f_o)$ with higher slopes and intercepts. Another trend of this relationship is characterized by geophones 2 and 5, with lower slopes and intercepts relative to the former. The two trends represent different geological backgrounds: the former is situated at limestone rocks, and the latter at quartzite or quartz-pebble conglomerate rocks. When seismic waves from source arrive at the different stations through different paths, the path effects, which implies the medium properties, have affected the observations of the seismic spectra.

As an average for 22 events at the Quirke failure zone, the slopes of plateau-frequency spectra at 5 sites are all greater than 3.0 in absolute values, of which the slopes of -3.8, -3.6 and -3.5 at sites 1, 3 and 5 are higher than the values of -3.2 and -3.3 at sites 2 and 4. The higher slopes reflect the properties of the fractured zone.

CONCLUSIONS

Although the sensor site responses may result in analytical deviations, which have been discussed, it does not affect the conclusions drawn below, being comparable with others.

1. The high P-wave energy at Quirke Mine, shown by E_p/E_T - 22%, which could be characteristic of the pillar bursts in the failure zone, and the high P-wave energy events are possibly events with a non-double couple focal mechanism.
2. The stress drop shows the various values ranged from 100 kPa to 5 MPa at Quirke, typical for mining-induced seismic events.
3. The ratio of f^P_o/f^S_o averaged about 1.69 and the higher slopes over 3.0 in absolute values are also the properties of the failure zone, which could be more associated with pillar bursts or induced burst events, and to some extent may be related to the pillar implosion.

4. Seismic moment ranged from about 50 to 2022 GN.m, and source radius ranged from about 30 to 90 m, which are comparable with those of mine tremors in the Ruhr Basin in Germany (43) and of the small tremors in Polish copper mines (41). Source radius increases and corner frequency decreases with increasing seismic moment in the condition of constant stress drop.
5. Peak particle velocities and accelerations presently observed are consistent with other mines in Northern Ontario.

ACKNOWLEDGEMENTS

This paper was completed under the supervision of Dr. D.G.F. Hedley of the Elliot Lake Laboratory, CANMET, Energy, Mines and Resources Canada. Messrs. P. Rochon, M. Plouffe and T.P. Lim provided great assistance in familiarizing me with the computer systems in the Laboratory. Dr. R. Tervo reviewed the manuscript and the office staff are thanked for their cooperation. This study was funded by NSERC.

REFERENCES

1. Hedley, D.G.F., Roxburgh, R.W. and Muppalaneni, S.N., "A case history of rockbursts at Elliot Lake"; Proc 2nd Int Conf Stability in Underground Mines, Lexington, Kentucky, 1984.

2. Labuc, V., Bawden, W. and Kitzinger, F., "Seismic monitoring system using fibre optic signal transmission"; Proc 6th Int Rock Mech Congr, Montreal, Quebec, 1987.

3. Semadeni, T., Rochon, P. and Niewiadomski, J., "Waveform analysis of mine induced seismic events recorded at Rio Algom's Quirke Mine"; Proc 2nd Int Symp Rockbursts and Seismicity in Mines, Minneapolis, Minnesota, pp 267-277, 1988.

4. Brune, J.N., "Tectonic stress and spectra of seismic shear waves from earthquakes"; J Geophys Res, vol. 75, pp. 4997-5009, 1970.

5. Brune, J.N., "Correction"; J Geophys Res, vol 76, p. 5002, 1971.

6. Salamon, M.D.G., "Rock mechanics of underground excavations"; Proc. 3rd Congr Int Soc Rock Mech, Denver, Colorado, pp. 951-1099, 1974.

7. Hanks, T.C. and Wyss, M., "The use of body-wave spectra in the determination of seismic source parameters"; Bull Seismol Soc Am, vol. 62, pp. 561-589, 1972.

8. Wyss, M. and Hanks, T.C., "The source parameters of the San Fernando earthquake inferred from teleseismic body waves"; Bull Seismol Soc Am, vol. 62, pp. 591-602, 1972.

9. Haskell, N., "Total energy and energy spectral density of elastic wave radiation from propagating faults"; Bull Seismol Soc Am, vol 54, pp. 1811-1842, 1964.

10. Berckhemer, H. and Jacob, K.H., "Investigation of the dynamical process in earthquake foci by analyzing the pulse shape of body waves"; Final Report. Contract Report AF61(052)-801, University of Frankfurt, Frankfurt, Germany, p. 85, 1968.

11. Savage, J.C., "Relation of corner frequency to fault dimensions"; J Geophys Res, vol. 77, pp. 3788-3795, 1972.

12. Sato, T. and Hirasawa, T., "Body wave spectra from propagating shear cracks"; J Phys Earth, vol. 21, pp. 415-431, 1973.

13. Dahlen, F.A., "On the ratio of P-wave to S-wave corner frequencies for shallow earthquake sources"; Bull Seismol Soc Am, vol. 64, p. 1159-1180, 1974.

14. Savage, J.C., "Relation between P- and S-wave corner frequencies in the seismic spectrum"; Bull Seismol Soc Am, vol. 64, pp. 1621-1627, 1974.

15. Hanks, T.C., "The corner frequency shift, earthquake source models and Q"; Bull Seismol Soc Am, vol. 71, pp. 597-612, 1981.

16. Silver, P., "Retrieval of source-extent parameters and the interpretation of corner frequency"; Bull Seismol Soc Am, vol. 73, pp. 1499-1511, 1983.

17. Trifunac, M.D., "Stress estimates for San Fernando, California, earthquake of February 9, 1971, main event and thirteen aftershocks"; Bull Seismol Soc Am, vol. 62, pp. 721-750, 1972.

18. Cook, N.G.W., "The application of seismic techniques to problems in rock mechanics"; Int J Rock Mech Min Sci, vol. 1, pp. 169-180, 1964.

19. Spottiswood, S.M. and McGarr, A., "Source parameters of tremors in a deep-level gold mine"; Bull Seismol Soc Am, vol. 65, pp. 93-112, 1975.

20. Hedley, D.G.F., "Rockburst terminology"; (in press) 1989.

21. McGarr, A., "Seismic moments and volume changes"; J Geophys Res, vol. 81, pp. 1487-1494, 1976.

22. Gutenberg, B. and Richter, C.F., "Magnitude and energy of earthquakes"; Ann Geofis, vol. 9, pp. 1-15, 1956.

23. Aki, K., "Generation and propagation of G-waves from the Niigata earthquake of June 16, 1964, 2, estimation of earthquake moment, released energy, and stress-strain drop from G-wave spectrum"; Bull Earthquake Res Institute, Tokyo University, vol. 44, pp. 73-88, 1966.

24. Brune, J.N., "Seismic moment, seismicity, and rate of slip along major fault zone"; J Geophys Res, vol. 73, pp. 777-784, 1968.

25. Hasegawa, H.S., "Lg spectra of local earthquakes recorded by the Eastern Canada telemetered network and spectral scaling"; Bull Seismol Soc Am, vol. 73, pp. 1041-1061, 1983.

26. Molnar, P., Tucker, B.E. and Brune, J.N., "Corner frequencies of P and S-waves and models of earthquake sources"; Bull Seismol Soc Am, vol. 63, pp. 2091-2104, 1973.

27. Masuda, T. and Takagi, A., "Source parameter estimates for small earthquakes" Sci Rep, Tohoku University, Ser. 5, Geophysics, vol. 25, pp. 39-54, 1978.

28. Rautian, T.G., Khalturin, V.I., Martynov, V.G. and Molnar, P., "Preliminary analysis of the spectral content of P and S-waves from local earthquakes in the Garm, Tadjikistan region"; Bull Seismol Soc Am, vol. 68, pp. 949-971, 1978.

29. Fletcher, J.B., "Spectra from high-dynamic range digital recordings of Oroville, California aftershocks and their source parameters"; Bull Seismol Soc Am, vol. 70, pp. 735-755, 1980.

30. Upadhyay, S.K. and Duda, S.J., "Source parameters of earthquakes from the Himalayan region"; J Geophys, vol. 48, pp. 67-79, 1980.

31. Rastogi, B.K. and Singh, D.D., "Source parameters of the Burma - India border earthquake of July 29, 1970, from body waves"; Tectonophysics, vol. 51, pp. T77-T84, 1978.

32. Kulhanek, O. and Meyer, K., "Source parameters of the Volvi - Langadhas earthquake of June 20, 1978, deduced from body-wave spectra at stations Uppsala and Kiruna"; Bull Seismol Soc Am, vol. 69, pp. 1289-1294, 1979.

33. Peppin, W.A. and Simila, G.W., "P- and SV-wave corner frequency over low-loss paths: a discriminant for earthquake source theories"; J Phys Earth, vol. 24, pp. 177-188, 1976.

34. Bakun, W.H., Bufe, C.G. and Stewart, R.M., "Body-wave spectra of central California earthquakes"; Bull Seismol Soc Am, vol. 66, pp. 363-384, 1976.

35. King, D. and Helmberger, D.V., "Time functions appropriate for some aftershocks of the point Mugu, California earthquake of February 21, 1973"; Bull Seismol Soc Am, vol. 65, pp. 127-132, 1975.

36. Burdick, L.J. and Helmberger, D.V., "Time functons appropriate for deep earthquakes"; Bull Seismol Soc Am, vol. 64, pp. 1419-1428, 1974.

37. Knopoff, L. and Mouton, J.O., "Can one determine seismic focal parameters from the far-field radiation?" Geophys J R Astr Soc, vol. 42, pp. 591-606, 1975.

38. Madariaga, R., "High-frequency radiation from crack (stress drop) models of earthquake faulting"; Geophys J R Astr Soc, vol. 51, pp. 625-651, 1977.

39. McGarr, A., Green, R.W.E. and Spottiswoode, S.M., "Strong ground motion of mine tremors - some implications for near-source ground motion parameters"; Bull Seismol Soc Am, vol. 71, No. 1, pp. 295-319, 1981.

40. Hanks, T.C., "Earthquake stress drops, ambient tectonic stresses and stresses that drive plate motions"; Pure Appl Geophys vol. 115, pp. 441-458, 1977.

41. Gibowicz, S.J., "The mechanism of seismic events induced by mining: a review"; Proc 2nd Int Symp Rockbursts and Seismicity in Mines, Minneapolis, Minnesota, 1988.

42. Hedley, D.G.F., "Peak particle velocity for rockbursts in some Ontario mines"; Proc 2nd Int Symp Rockbursts and Seismicity in Mines, Minneapolis, Minnesota, 1988.

43. Gibowicz, S.J., Harjes, H.P. and Schäfer, M., "Source parameters of seismic events at Heinrich Robert Mine, Ruhr Basin, Federal Republic of Germany: evidence for nondouble-couple events"; Bull Seismol Soc Am, vol. 80, pp. 88-109, 1990.

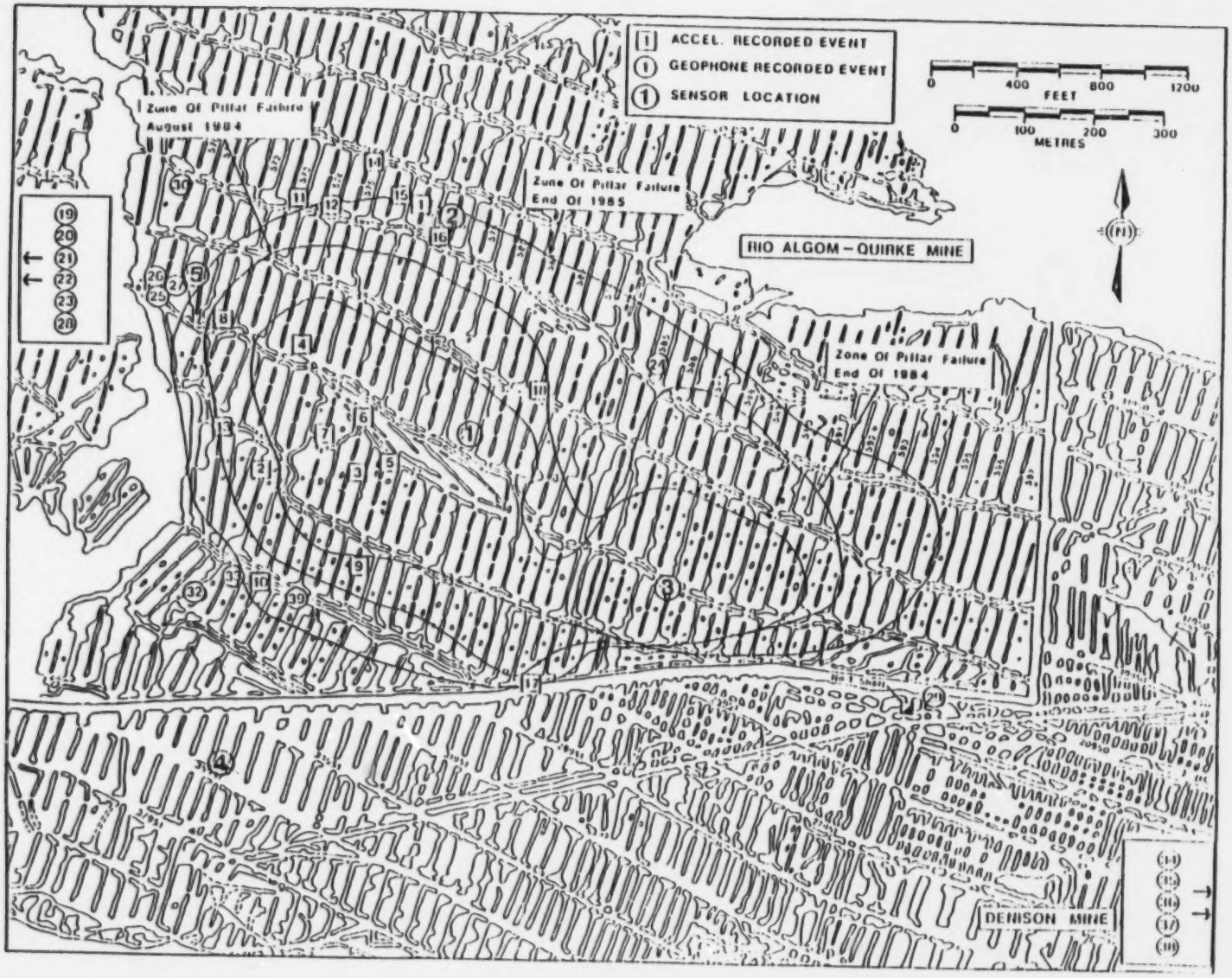

Fig. 1 - Plan view of Quirke Mine showing extent of failed zone, sensor and seismic event locations.

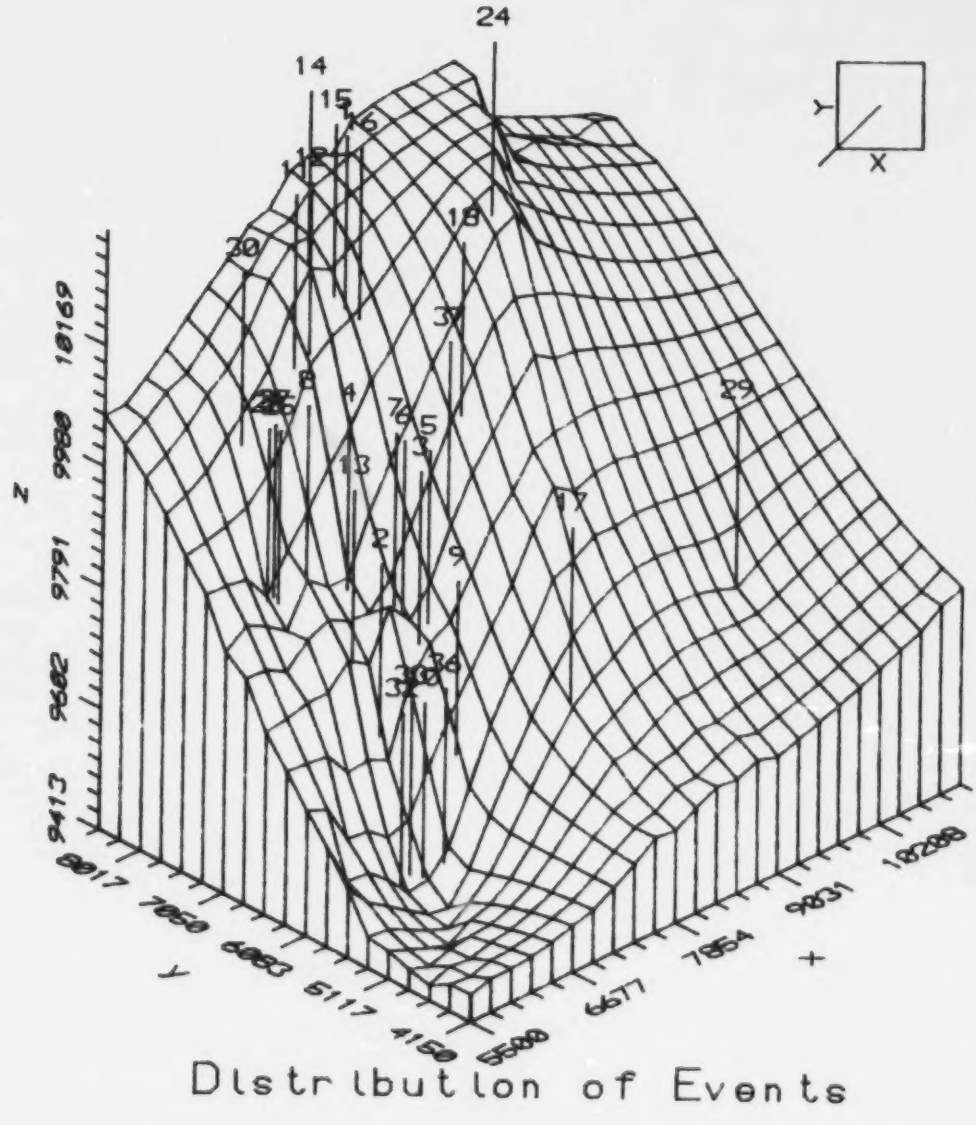

Fig. 2 - A stereogram of rockburst event locations at Quirke Mine and its adjacent areas in 1987.

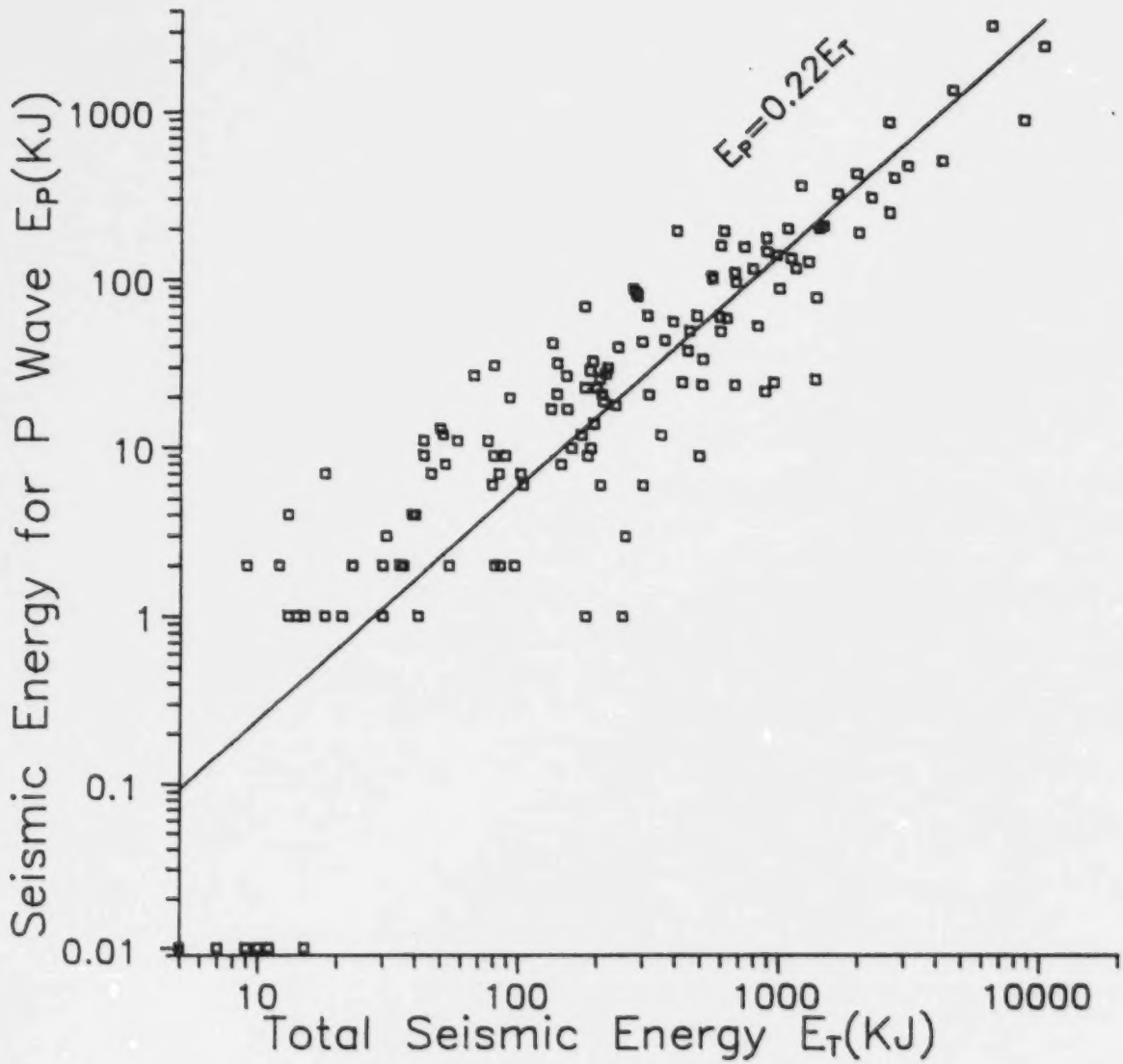

Fig. 3 - Proportion of seismic energy in P-wave at Quirke Mine.

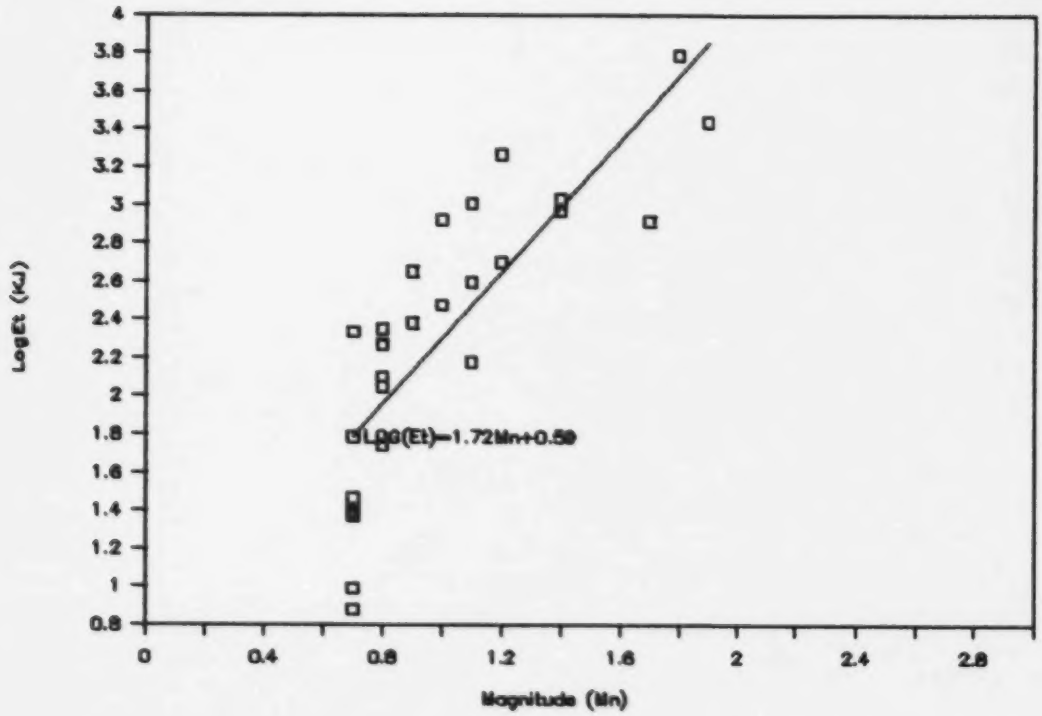

Fig. 4 - Seismic energy as a function of magnitude at Quirke Mine.

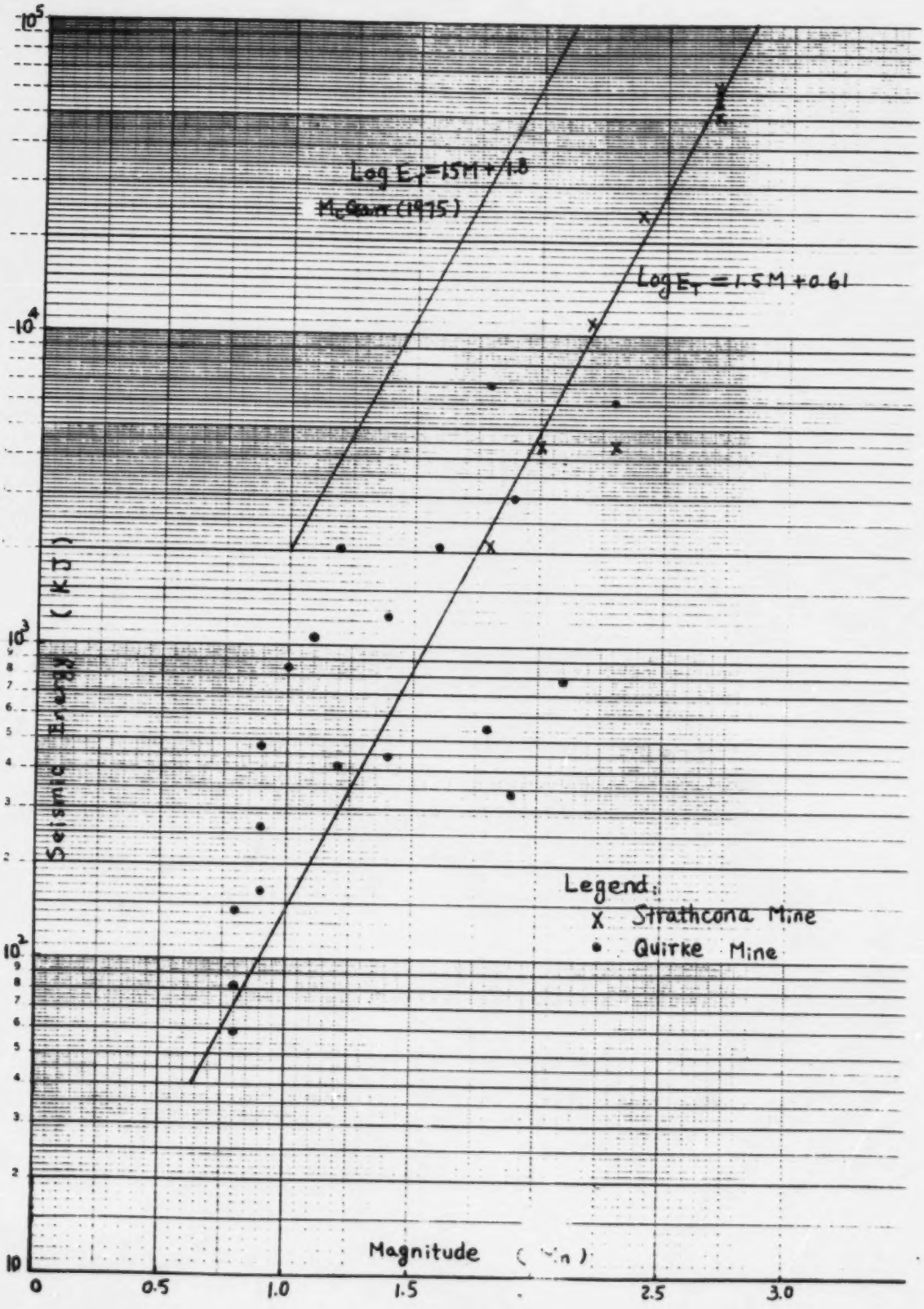

Fig. 5 - Relationship between seismic energy and magnitude (Strathcona Mine measurement from (20)).

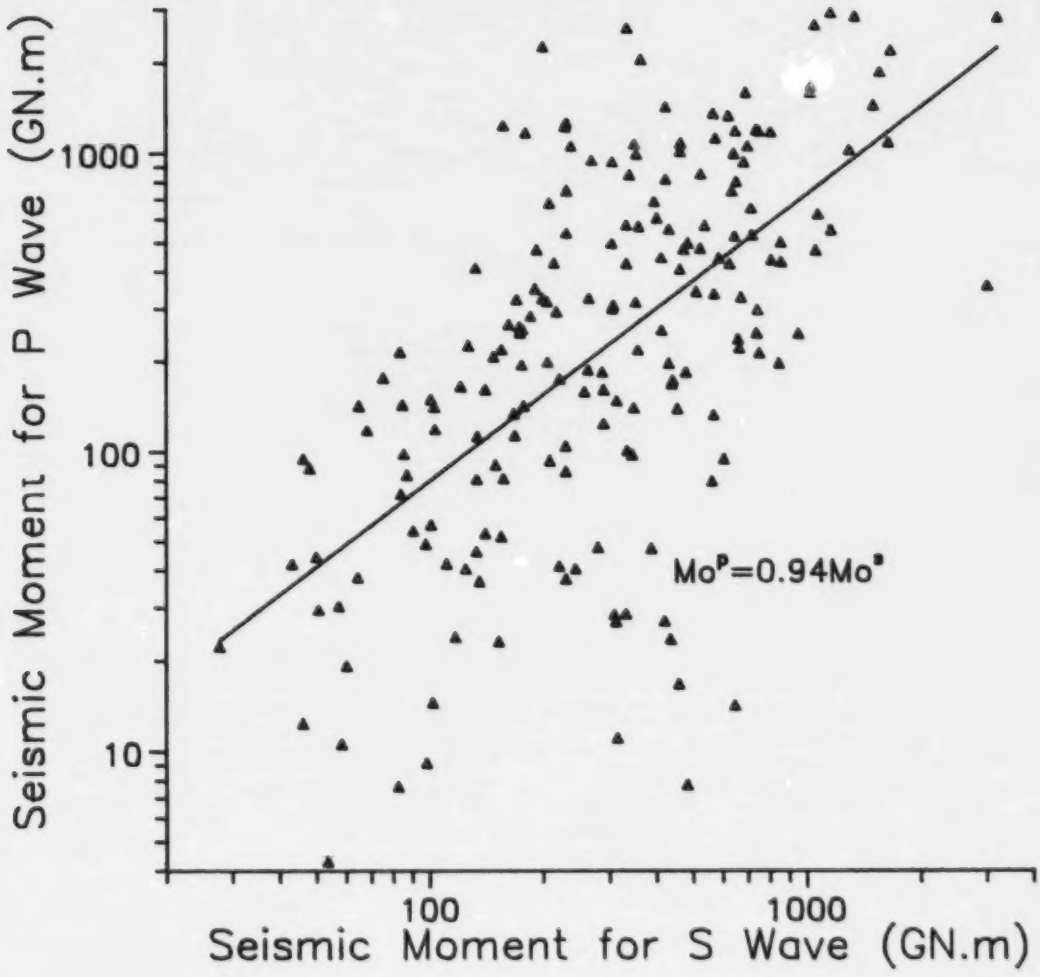

Fig. 6 - Relationship between the seismic moments for P- and S-waves at Quirke Mine and adjacent areas.

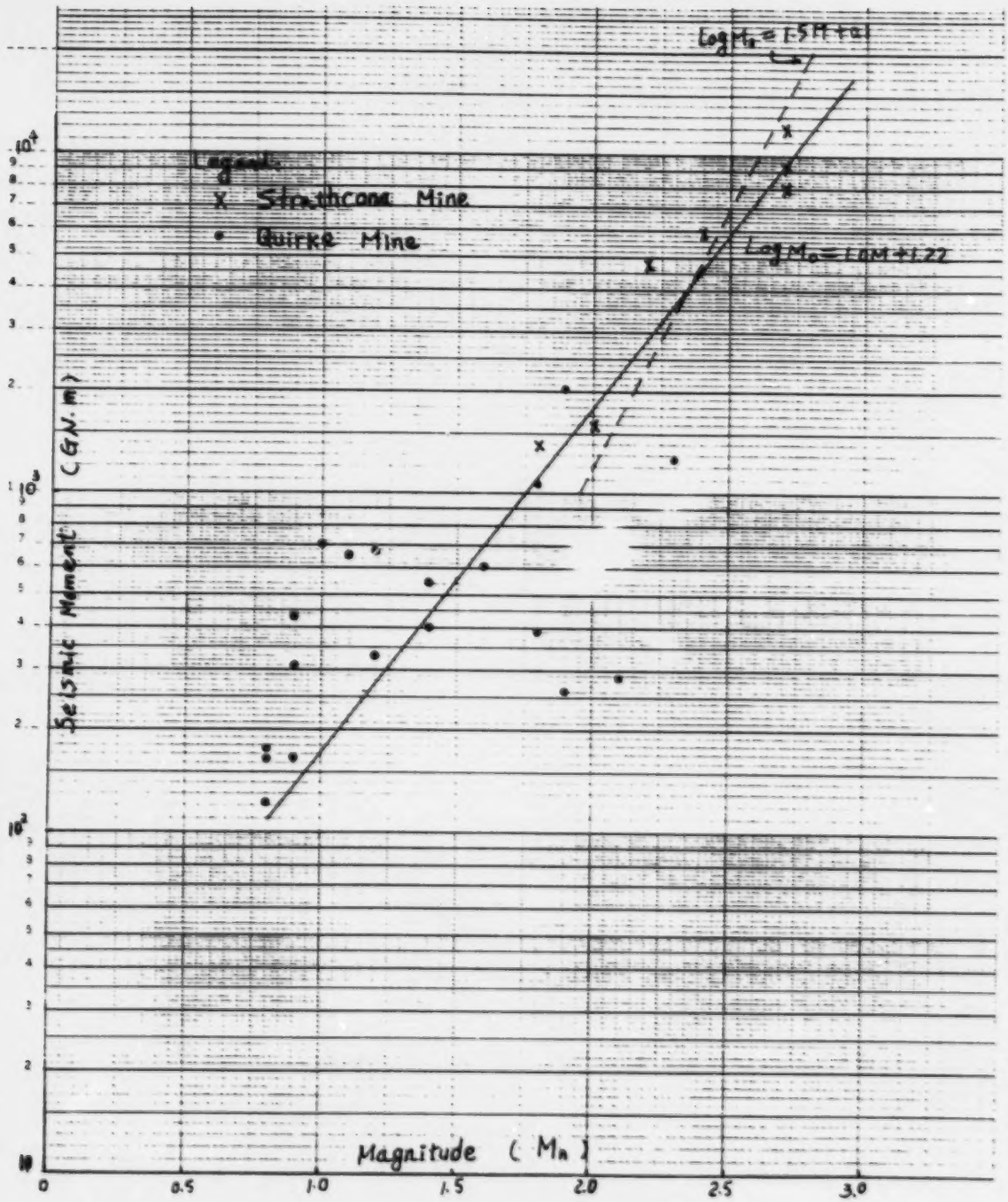

Fig. 7 - Relationship between seismic moment and magnitude at Quirke and Strathcona mines.

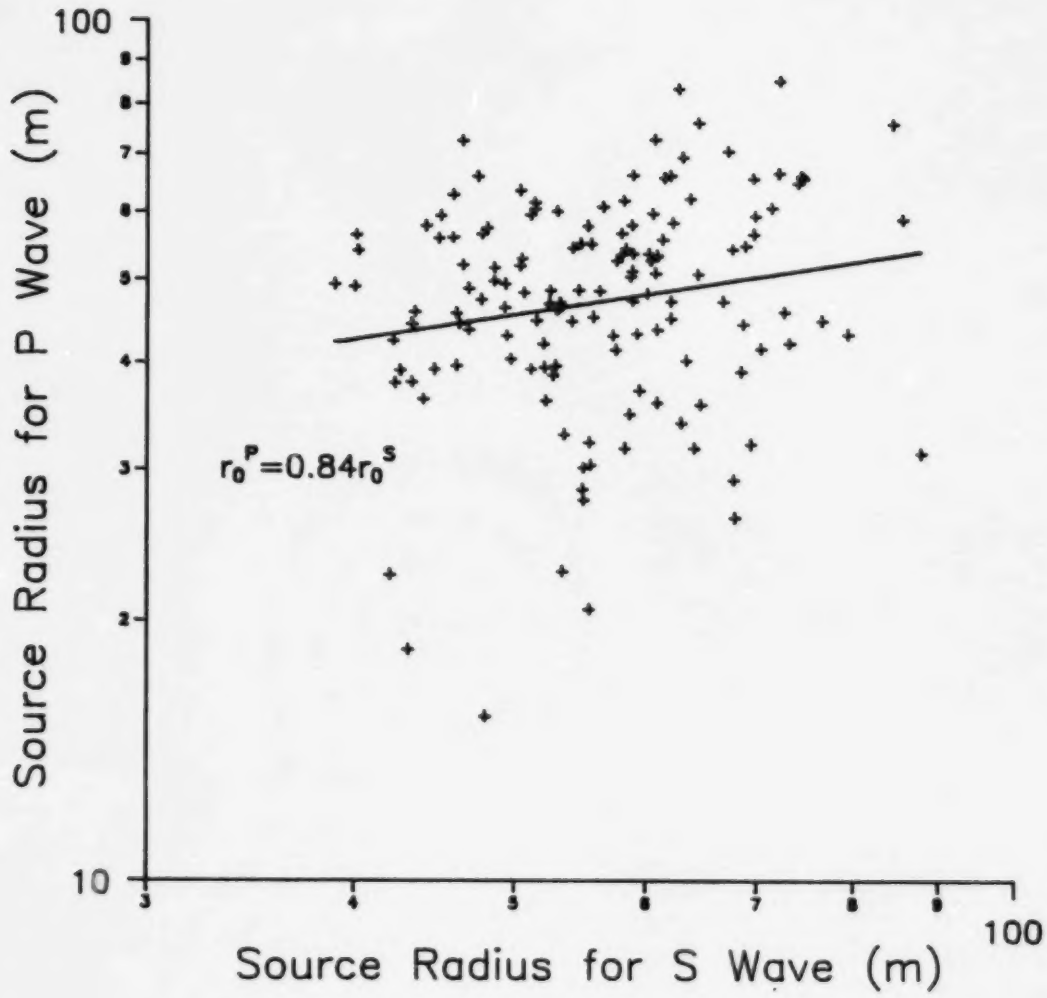

Fig. 8 - Relationship between the source radius for P- and S-waves at Quirke Mine.

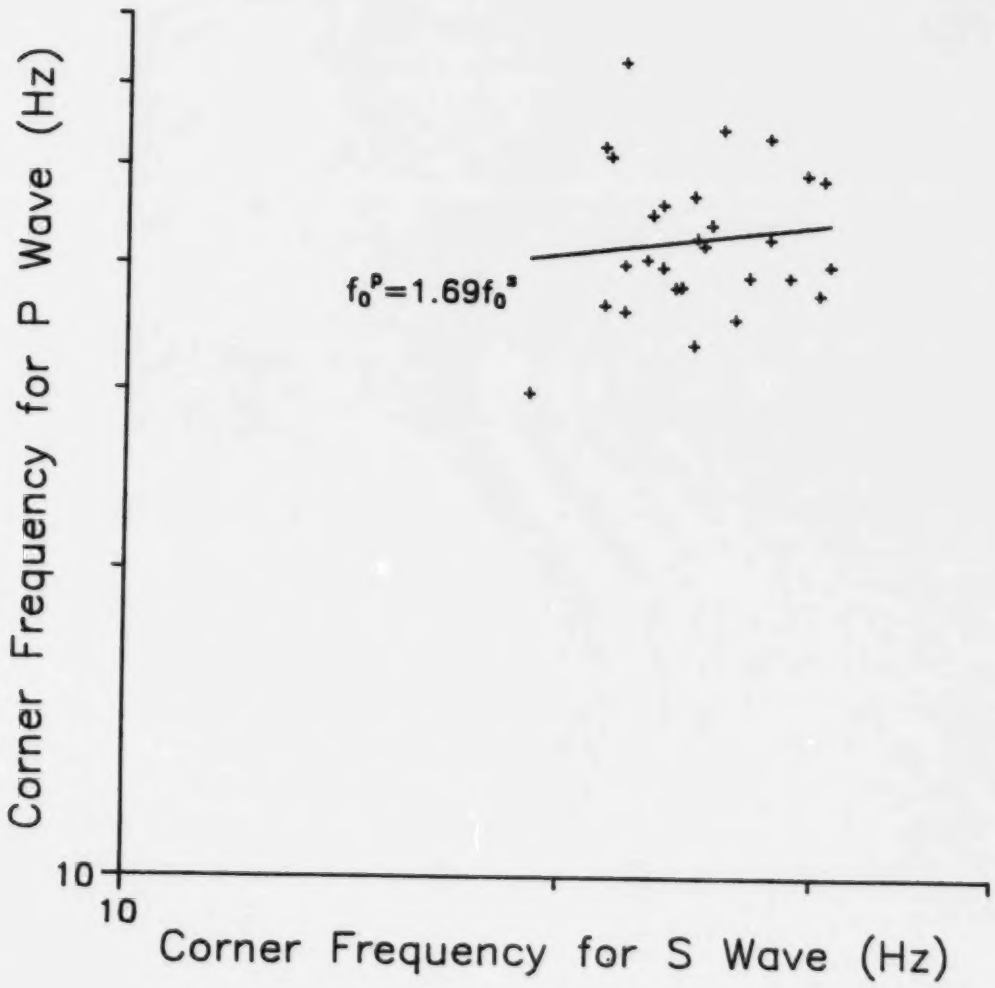

Fig. 9 - Relationship between P- and S-wave corner frequencies in the seismic spectra at Quirke Mine.

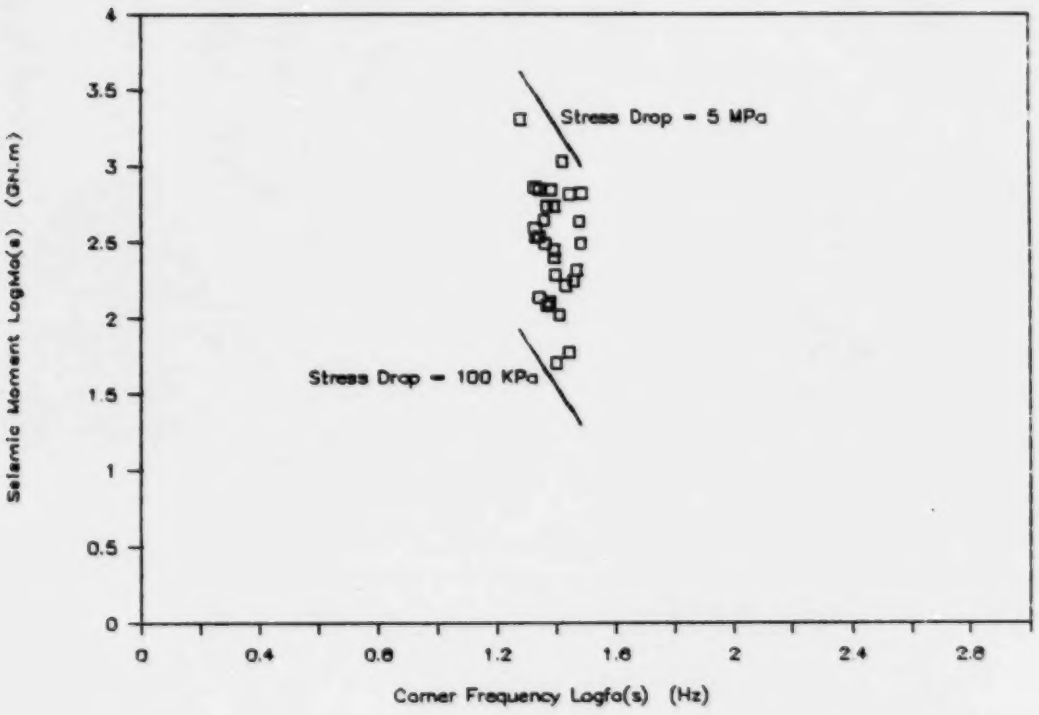

Fig. 10 - Seismic moment as a function of corner frequency at Quirke Mine.

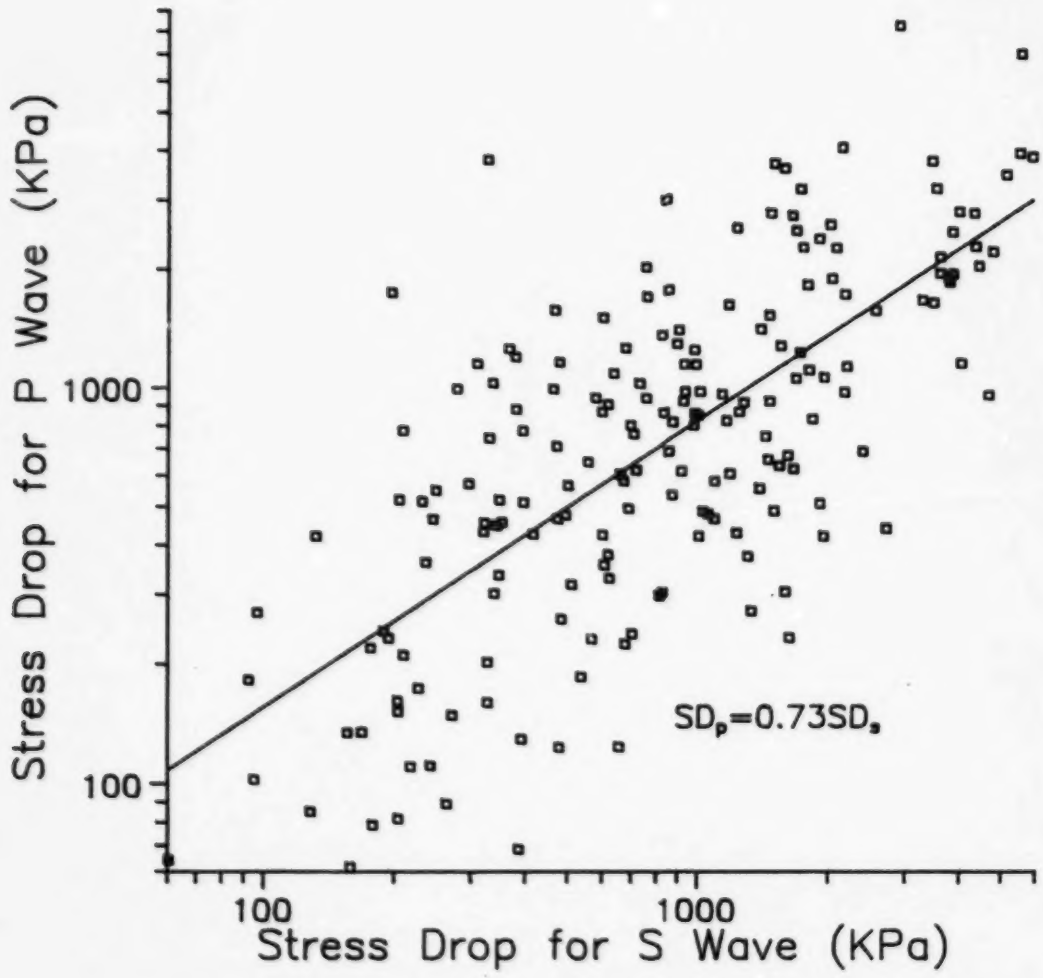

Fig. 11 - Relationship between stress drops for P- and S-waves at Quirke Mine.

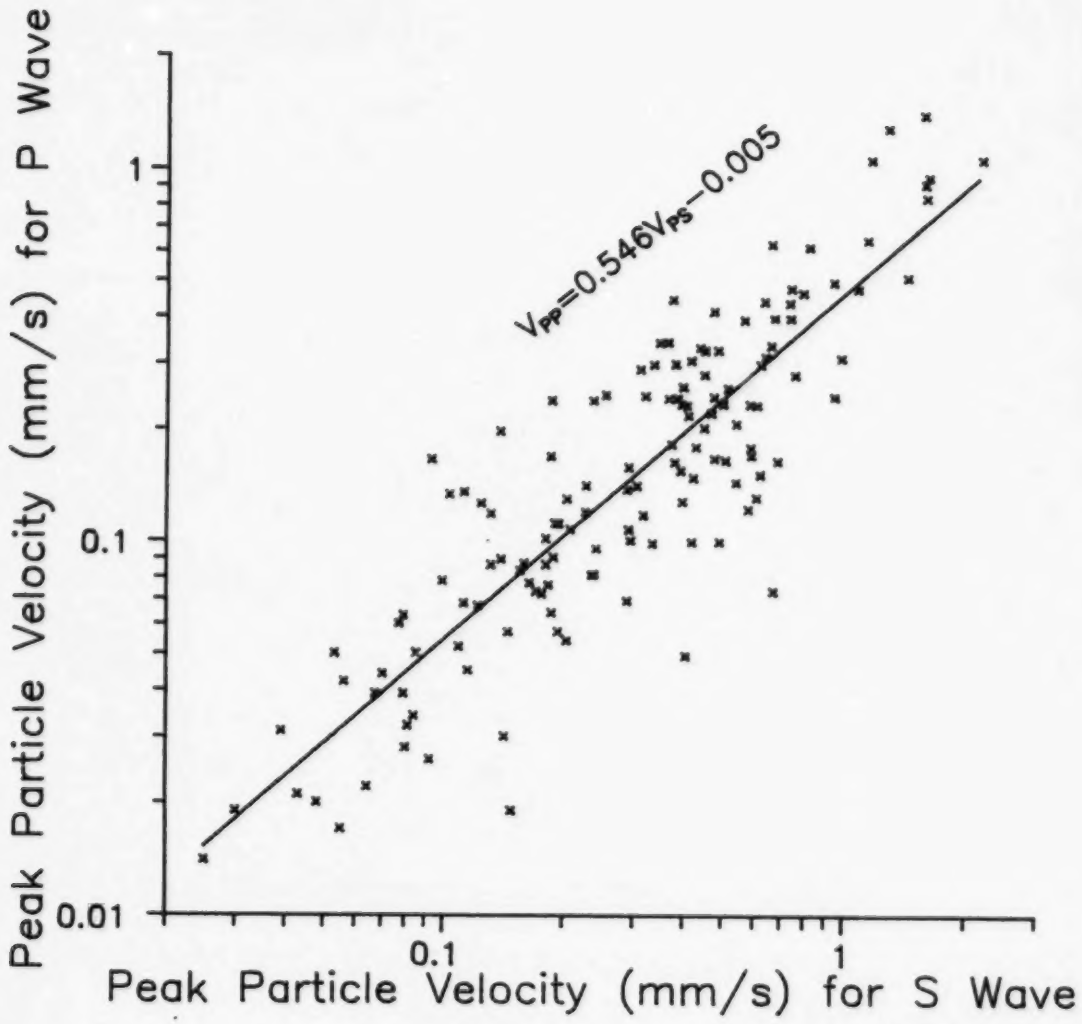

Fig. 12 - Relationship between the peak particle velocities for P- and S-waves at Quirke Mine.

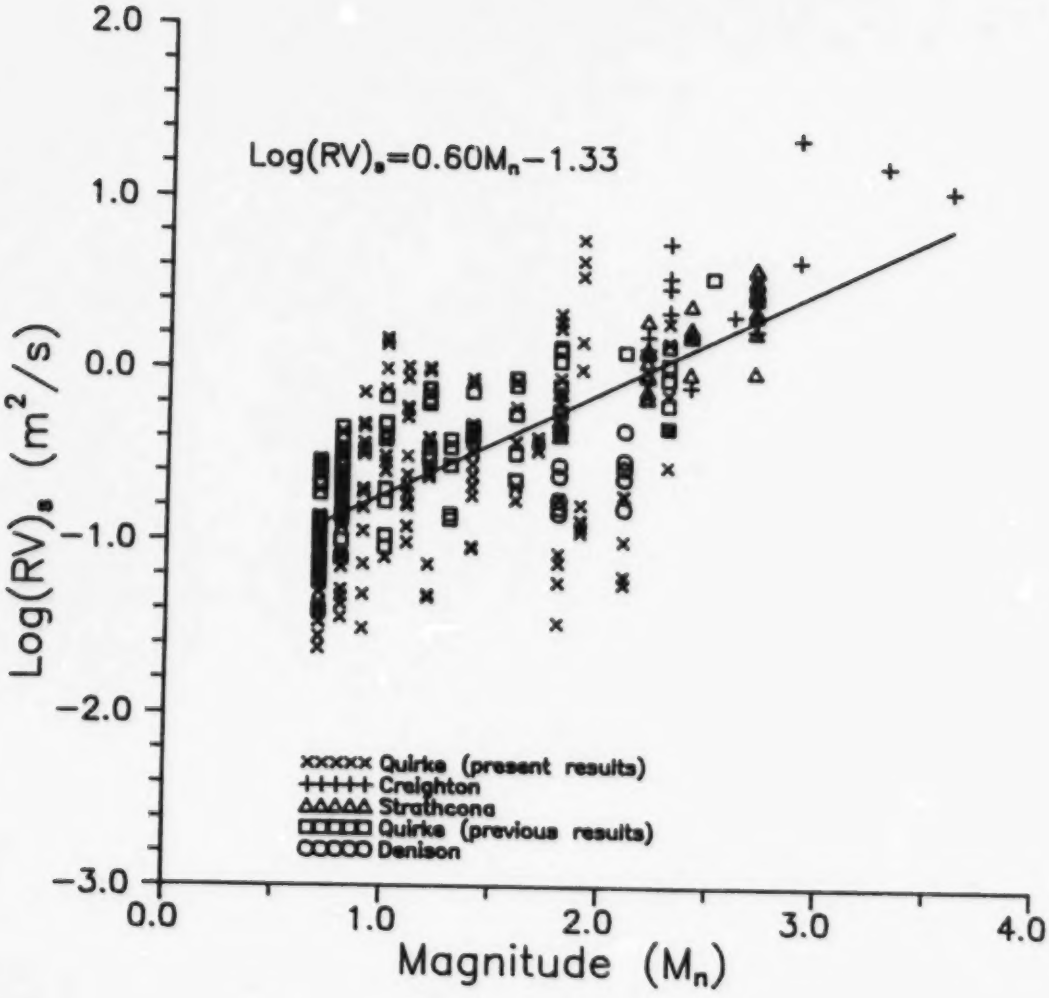

Fig. 13 - Scaled peak particle velocity as a function of rockburst magnitude, using a seismology format.

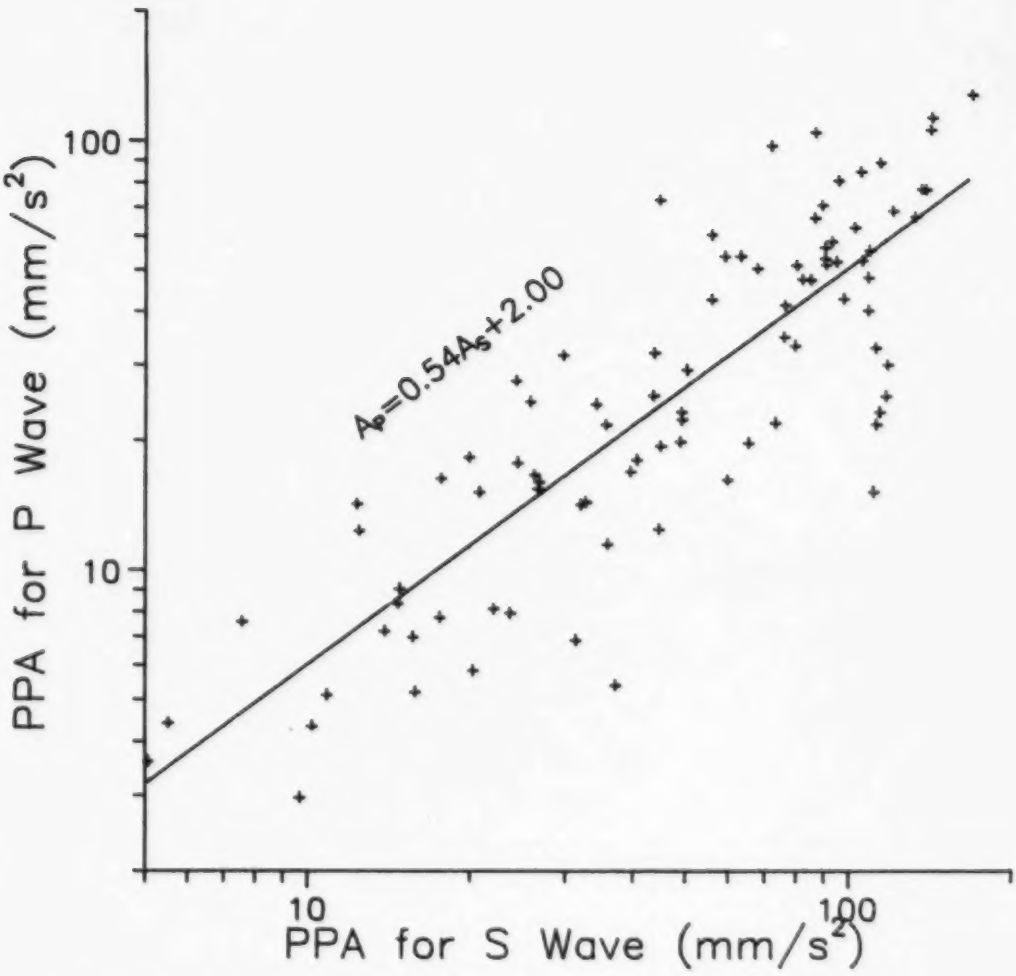

Fig. 14 - Relationship between the peak particle accelerations for P- and S-waves at Quirke Mine.

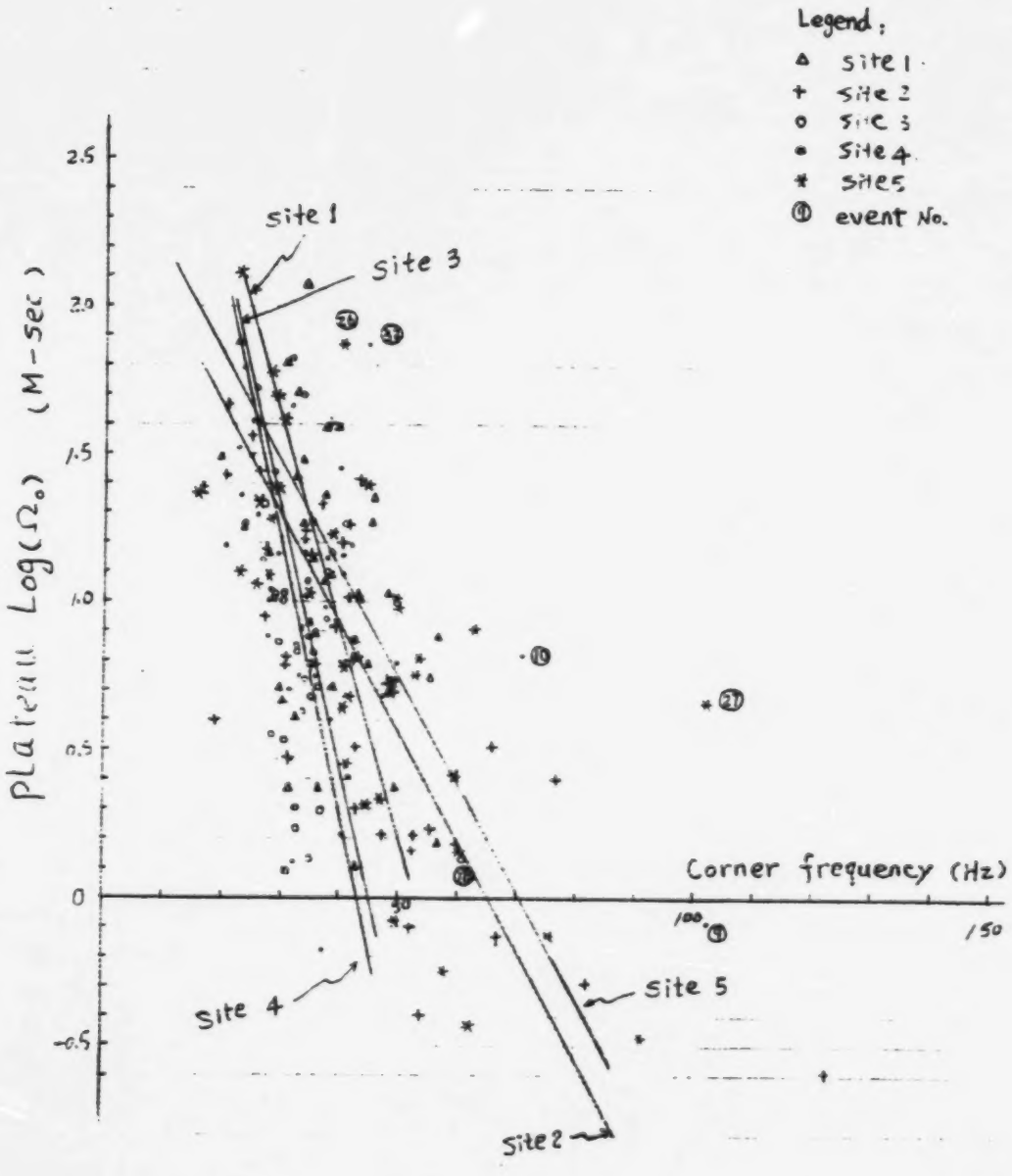

Fig. 15 - Log(Ωo) as a function of f_c at Quirke Mine.